Influence of bubbles on scattering of light in the ocean

Xiaodong Zhang, Marlon Lewis, and Bruce Johnson

The scattering and backscattering properties of bubble populations in the upper ocean are estimated with Mie theory and a generalized bubble size spectrum based on *in situ* observations. Optical properties of both clean bubbles and bubbles coated with an organic film are analyzed; the results are compared with the corresponding optical properties of micro-organisms of similar size. Given a bubble number density (from $\sim 10^5$ to $\sim 10^7$ m^{-3}) frequently found at sea, the bubble populations significantly influence the scattering process in the ocean, especially in oligotrophic waters. Bubbles appear to make a large contribution to the missing terms in constructing the observed total backscattering coefficient of the ocean. This contribution to backscattering is strongly enhanced if the bubbles are coated with organic film. The injection of bubbles will shift ocean color toward the green, resembling phytoplankton blooms, and hence introducing error in ocean color remote sensing if its effect is not corrected. © 1998 Optical Society of America

OCIS codes: 010.4450, 290.0290, 290.1350.

1. Introduction

Satellite observations of the color of the ocean's surface, as exemplified by the Coastal Zone Color Scanner, the Ocean Color and Temperature Sensor, and the Sea-Viewing Wide Field-of-View Sensor (SeaWiFS), have transformed perceptions of biological variability in the sea and have established the feasibility of using remote sensing for estimation of marine primary productivity and biogeochemical fluxes over large areas synoptically and over long time periods.[1–3] For this approach to be successful, accurate interpretations of the biological and physical processes responsible for variations in the color of the ocean are crucial.

Applications of ocean color remote sensing depend on the spectral variation in the diffuse reflectance of the surface ocean, $R(\lambda)$, which is in turn related to the ratio of the backscattering coefficient $b_b(\lambda)$ (m^{-1}) to the absorption coefficient $a(\lambda)$ (m^{-1}),[4,5]

$$R(\lambda) = f[b_b(\lambda)/a(\lambda)], \quad (1)$$

where f is a parameter that depends on the illumination conditions (e.g., solar zenith angle and cloud cover) as well as the water optical properties (e.g., single-scattering albedo and ratio of molecular backscattering to that caused by particles).[6–8] For case 1 waters,[5] several semianalytical models have been established to relate absorption and backscattering coefficients to the desired chlorophyll concentration [Chl].[9,10] Although variations in the absorption coefficient that are primarily due to variation of pigment concentration[11,12] modify the underwater light field, it is backscattering, ultimately, that determines how much light is reflected by the ocean and then observed by satellite.

For scattering and backscattering, however, there is large variance (50–200%) about the empirical relationships between these coefficients and pigment concentration.[6,9,10] Theoretical calculations and laboratory observations[13,14] have found that living algae have a negligible influence on the backscattering process by oceanic waters. Moreover, recent theoretical and laboratory studies on the optical properties of both phototrophic and heterotrophic plankton have indicated that, whereas microorganisms, particularly phytoplankton and heterotrophic bacteria, could account for most of the total scattering in clear waters, they contribute only a small fraction of the observed backscattering.[15–17] These studies postulated that unidentified submicrometer particles (~ 0.1 μm) with low ($n < 1.03$), but also possibly high, refractive index might be required to explain the large portion of the total particulate backscattering that is unaccounted for by microorganisms, a conjecture that was previously suggested by Brown and Gordon[18,19] who tried but failed to use Mie theory to predict the observed volume scattering function of particles in the Sargasso Sea.

The authors are with the Department of Oceanography, Dalhousie University, Halifax B3H 4J1 Canada.

Received 2 February 1998; revised manuscript received 8 June 1998.

0003-6935/98/276525-12$15.00/0

Table 1. Bubble Experiments and Their Statistical and Optical Characteristics

Number	Reference	Date	Method	Region	Wind Speed (ms^{-1})	N_0 (m^{-3})	PDF[a]	$r_{min}/r_a - r_b$[b]	Slope[c]	$\bar{r}$ (μm)	$\bar{s}$ (μm^2)	$b(m^{-1})$[d]	$b_b(m^{-1})$[d]
1	26	February	Acoustic	Monterey Bay, Calif.	0	9.1×10^4	DII	18	2–4	27.5	2.83×10^3	5.16×10^{-4}	5.99×10^{-6}
2	28	June	Photograph	North Atlantic	11–13	4×10^4	DI	60–70	3.5	79	2.4×10^4	1.92×10^{-3}	2.23×10^{-5}
3	27	June	Acoustic	Monterey Bay, Calif.	0	1×10^6	DII	22	2–4	33	4.57×10^3	9.14×10^{-3}	1.06×10^{-4}
4	20	April	Photograph	St. Margaret's Bay, Nova Scotia	11–13	4.8×10^5	DI	40–50	4.5	52	1.1×10^4	1.05×10^{-2}	1.22×10^{-4}
5	52	October	Acoustic	Monterey Bay, Calif.	11	4×10^5	DI	40–50	4	52	1.1×10^4	8.80×10^{-3}	1.02×10^{-4}
6	39	August	Photograph	Tasman Sea, N.Z.	14	6.59×10^5	DI	68–85	3–6	110	4.57×10^4	6.02×10^{-2}	6.98×10^{-4}
7	22	August	Holograph	Santa Catalina Island, Calif.	0	2.13×10^7	DII	10	4	15	9.14×10^2	3.89×10^{-2}	4.51×10^{-4}
8	21	—	Acoustic	Open ocean	12–15	1.4×10^6	DII	30	2–4	56	1.39×10^4	3.95×10^{-2}	4.62×10^{-4}

[a]PDF, probability density function. DI is peaked distribution, DII is unpeaked distribution.
[b]For PDF = DI, it gives the peak position r_a and r_b [Eq. (4)], for PDF = DII, it gives the minimum radius r_0 (m) [Eq. (5)].
[c]For PDF = DI, it gives the slope of the log–log function of number density versus size for $r > r_b$.
[d]Estimated based on clean bubbles.

However, the submicrometer particles with either low or high refractive index have not been physically or chemically characterized, nor have their optical properties been determined; the missing terms in the backscattering process remain enigmatic.

Here we hypothesize that backscattering by air bubbles in the ocean, which can often be found present in abundance,[20,21] even in quiescent seas,[22] can in large part account for these missing terms.

Air bubbles in the ocean are generated mainly by injection of air by breaking waves.[23] These bubbles play important roles in gas transport between atmosphere and the ocean,[24,25] underwater sound interference through scattering and absorption,[26,27] and formation of marine sea-salt aerosols.[28–30] Bubbles also influence the light propagation in water where they are present. Marston and co-workers examined the light scattering near the critical angle (82.8°), Brewster angle (106.2°), and glory (180°) for a single bubble.[31–36] The bulk optical properties, such as scattering and backscattering coefficients of a bubble population, which might be quite different from those of a single bubble, however, have not been studied extensively.

Pioneering research on the bulk optical properties of bubbles in the ocean was carried out by Stramski,[37] who studied the light-scattering capability of clean bubble populations with a size distribution following the −4th power law for radii between 10 and 150 μm. He found that this class of bubbles can contribute as high as approximately 10% to the scattering and backscattering coefficients of seawater. He used the bubble size distribution measured by O'Hern *et al.*[22] using a holographic method. This bubble size distribution assumes that the bubble number decreases as size increases according to the −4th power law, agreeing with the acoustical observation in general shape. However, many *in situ* measurements[20,38–40] have observed bubble size distributions with a plateau located somewhere between 40 and 80 μm (Table 1, column 9). Although it has been argued that these peaked distributions are an artifact of the optical methods used,[21] there is still uncertainty in the reasons for differences between optical and acoustical results. The light scattering that is due to bubble populations with such a size distribution vary from the situation analyzed by Stramski. Furthermore, Stramski considered only clean bubbles; in nature, bubbles acquire organic films quickly after their formation in the sea.[24] These organic films are composed mainly of protein or lipid,[41] whose mean relative refractive indices ($m = 1.20$ for protein and $m = 1.10$ for lipid) are quite different from that of air bubbles ($m = 0.75$), and thus it is expected that the coated bubbles would scatter somewhat differently from clean bubbles.

To address our hypothesis that we raise in this paper, we adopt an approach similar to that used by Stramski.[37] However, we use a generalized bubble size distribution based on all the available *in situ* bubble measurements in the ocean. Then we focus on the effect of organic film adsorbed onto the bubble surface on the optical properties of bubble populations. Finally, the influence of the presence of bubbles on the remote sensing of ocean color is evaluated.

2. Background and Bases

The bulk optical properties of the bubble population are calculated as

$$j = \int_{r_{min}}^{r_{max}} Q_j(r)\pi r^2 n(r)\mathrm{d}r, \tag{2}$$

where j denotes either b (m^{-1}) (total scattering coefficient) or b_b (m^{-1}) (backscattering coefficient). Correspondingly, Q_j is the dimensionless efficiency factor, calculated with Mie theory,[42,43] for single-bubble scattering and backscattering. The $n(r)$ ($m^{-3}\ \mu m^{-1}$) is the bubble size distribution, representing the bubble number per unit volume per unit ra-

dius interval at radius r. The r_{min} and r_{max} denote the minimum and maximum radius of the bubble population. In our calculations, the r_{max} is set to be 300 μm, which roughly corresponds to the maximum radius found in most field experiments. The r_{min} of the bubble population in the sea that has been observed so far is 10 μm by use of holographic techniques.[22] An even smaller radius (~3 μm) for stable bubbles was suggested by the results of Johnson and Cooke.[44] The study by Yount *et al.*[45] found stabilized bubbles in both distilled water and gelatin of radius of the order of 1 μm or less. Finally the gas cavitation nuclei has an estimated radius of ~0.1 μm.[46] In our calculations, the r_{min} is set to be 0.01 μm.

The bubble size distribution $n(r)$ at radius r can be expressed as

$$n(r) = N_0 p(r) \ (\mathrm{m}^{-3}\ \mu\mathrm{m}^{-1}), \tag{3}$$

proportional to where N_0 (m^{-3}) is the total bubble number density in a unit volume of water and $p(r)$ ($\mu\mathrm{m}^{-1}$) is the bubble probability density function (PDF) at radius r. From Eqs. (2) and (3), it is clear that bubble optical properties are directly proportional to bubble number density. For bubbles generated by breaking waves, both theoretical analyses[47,48] and field experiments[49] suggest that N_0 depends on wind speed through an empirical power law, i.e., $N_0 \propto U_{10}{}^{\alpha}$. The exponent α ranges from 3.0 to 4.7 when U_{10} is given in meters per second. On the other hand, a background bubble population[50] can also be found in calm seas.[22,27] These bubbles are believed to be possibly of biological origin[26] or from decay of wind-generated bubble patches.[50] The N_0 observed *in situ* is listed in Table 1 along with the experimental conditions. The N_0 ranges from 4×10^4 to 2×10^7 (m^{-3}). Despite the intrinsic limitations of various methods used to observe bubbles,[51] in the following study the bubble number density N_0 is assumed to vary from 10^4 to 10^8 (m^{-3}) to represent the full-range of bubble populations found in the sea, without regard to the specific generating mechanism.

Once bubble clouds are formed, the bubbles evolve by such processes as dissolution, rise, and gas expansion, all of which are a function of bubble size. Therefore these processes regulate the bubble PDF with respect to size. The *in situ* observations support, in general, two types of bubble density functions (Table 1, column 8). One has a plateau with the bubble concentration dropping off rapidly on both sides of the plateau (denoted here as DI). The other exhibits a monotonic increase as the bubble radius decreases (DII). The bubble size distributions obtained by optical methods and simulated by numerical models seem to support DI; however, the peak positions are different in different observations. DII, on the other hand, agrees with most acoustical observations. The common features between DI and DII is that both admit a power-law decrease of bubble number density with increasing radius (larger than peak for DI), with the mean exponent being −4.[30,39,49]

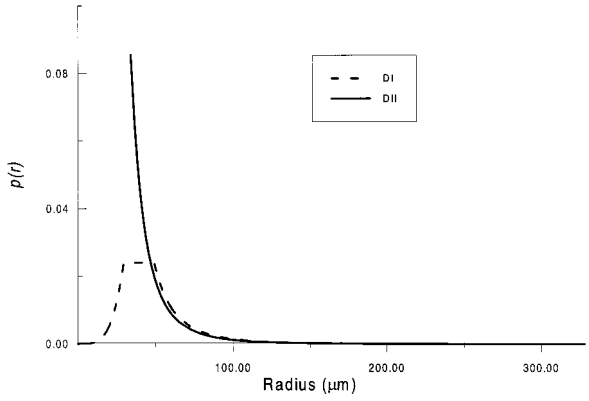

Fig. 1. Schematic plot of two representative bubble size distributions frequently found in the ocean. The figure is plotted such that the two distributions have the same mean radius of 50 μm. For the DI (dashed curve), the plateau is located between 30 and 50 μm, and for the DII (solid curve) the minimum radius is approximately 34 μm.

Crawford and Farmer[52] and Wu[48] gave two, similar, expressions to describe the DI bubble size spectrum on the basis of Johnson and Cooke's *in situ* observations.[20] Based on their results, here we give a more generalized bubble PDF for DI, the particular form of which depends on the peak position:

$$p(r) = \begin{cases} c_1 r^4 & 0 \le r < r_a \\ c_2 & r_a \le r < r_b \\ c_3 r^{-4} & r_b \le r \end{cases}, \tag{4}$$

where r_a and r_b are the radii of bubbles that define the limits of the plateau and c_1, c_2, and c_3 are uniquely determined by r_a and r_b.

The bubble size distributions of the DII type are proportional, on the average, to r^{-4} over the entire range. It is obvious that this relationship cannot be extended to zero radius; this would imply an infinite volume of gas inside the bubbles. The radius corresponding to the maximum bubble density is not known. For the DII density function, the generalized form is

$$p(r) = c\, r^{-4} \quad r \ge r_0, \tag{5}$$

where r_0 is the minimum radius for DII distribution and c depends only on r_0. Note that the r_0 here is the minimum radius for DII distribution only. It is a variable in the following analysis, whereas r_{min} of Eq. (2) is a constant, defining the smallest radius down to which the Mie calculation and bubble size distribution extend. In case $r_0 > r_{min}$, the $p(r)$ of Eq. (5) is set to be 0 for $r_{min} < r < r_0$. Figure 1 is a schematic plot of DI and DII with the same mean radius at 50 μm.

In the bubble size spectra we have used, a mean exponent -4 [$p(r) \sim r^{-4}$, Eqs. (4) and (5)] is adopted. It was found that a higher exponent, i.e., −3 or −2, might be associated with the biologically generated bubbles.[27,53] In reference to Eq. (2), it is straightforward to show that for $\xi \le 3$, where $p(r) \sim r^{-\xi}$, the

integral of Eq. (2) would be $\ln(r)$ if $\xi = 3$ or r if $\xi = 2$, the values of which depend on r_{max} (because Q_j is almost constant for large size bubbles). In other words, the optical properties of bubbles of biological origin would be largely determined by large bubbles. Because these bubbles of biological origin are usually thought to be present in low number density, their influence is likely to be small, except in coastal environments or in bloom conditions.

3. Results and Discussions

A. Optical Efficiencies for Single Bubble

As stated above, natural bubbles are always coated with organic materials and adsorbed particles. Here we expand the analysis of Stramski[37] to consider dirty bubbles coated with a surface-active monolayer. Unlike the particles that may adsorb onto bubbles,[54] photographs show that bubbles with adsorbed monolayers remain spherical.[44] However, the composition and thickness of coatings are not clearly known. Fox and Herzfeld[55] suggested that protein might be the source of the monolayer coating the bubble. Yount[46] suggested both protein and lipid as components of the film. Therefore in this study we use both. The thickness of such coatings for bubbles in seawater has been estimated to range from 0.01 μm for lipids such as fatty esters, fatty acids, and fatty alcohols, to 1 μm for proteinaceous molecules such as glycoproteins and proteoglycans.[41] For the bubble cavitation nuclei in gelatin, the thickness of this layer is within 5–50 Å.[46] A single layer of monomolecular film of constant thickness is assumed here regardless of bubble radius. This assumption might not be realistic, but it represents a compromise situation for the dirty bubble. The large bubbles are only partly coated by organic film,[24] and only as the bubbles contract and become small enough can this film then form a complete skin[55]; on the other hand, as bubbles age, the film thickness grows and the absorbed film can turn into a multilayered system.[41]

Figure 2 shows the variation of (a) scattering and (b) backscattering efficiency with bubble size ($\lambda = 550$ nm) and as a function of film thickness for bubbles coated with a protein monolayer (refractive index 1.2). The thickness of the film was assumed to vary from 0 (clean bubbles) to 1 μm. A common feature for coated bubbles is that both scattering and backscattering efficiencies first decrease to a minimum (the thinner the film, the sharper the decrease), then increase reaching a global maximum, and after that it oscillates toward asymptotic values as bubble sizes become large relative to wavelength. This is in contrast to clean bubbles, whose scattering function of size reaches a maximum first.

For bubbles sizes larger than 10 μm ($\lambda = 550$ nm), the variations in total scattering efficiency that are due to coatings become small (<10%), and there is little difference between clean and dirty bubbles. For the backscattering efficiency, however, the situation is quite different [Fig. 2(b)]. Organic film coatings enhance the backscattering efficiency after the first maximum, and the enhancement depends directly on the

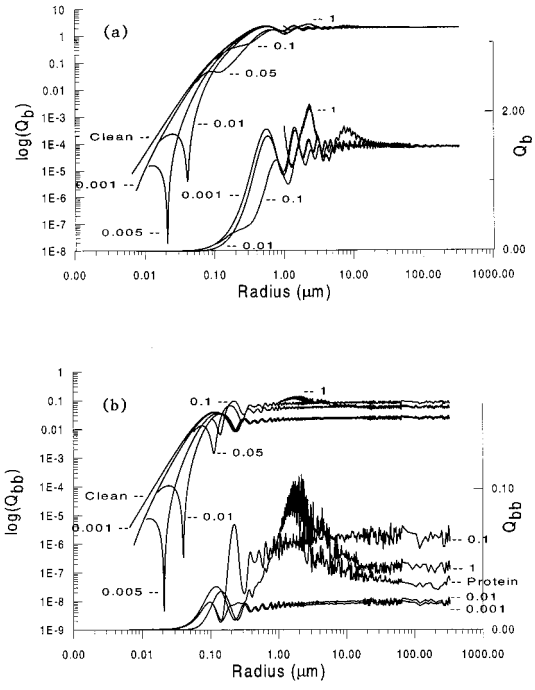

Fig. 2. Variations of (a) scattering and (b) backscattering efficiency with bubble size and as a function of thickness of a protein film. To identify the variations for both small and large sizes, the same data set is plotted in logarithmic scale (left) and linear scale (right). The efficiencies for bubbles with a film of various thicknesses are indicated by the thickness (in micrometers), whereas clean denotes the efficiency for clean bubbles and protein refers to a homogeneous protein sphere of the same size as bubbles.

thickness of the coated films. There is no significant variation in backscattering for film thickness of <0.01 μm; however, it increases four fold as the film further thickens to 0.1 μm. An exception is for bubbles with a much thicker film (~1 μm), which after the first maximum the efficiency decreases as bubble size increases (>10 μm), reaching a value even smaller than that for bubbles with 0.1-μm film. It resembles the backscattering efficiency distribution for protein sphere (presumably a spherical protein of the same size as bubbles) in shape, but with a somewhat higher magnitude. Further increasing the film thickness (up to 5 μm as we tested, and the result is not shown) does not change the pattern of backscattering much from that for a film of 1-μm thickness.

It is clear from Figs. 2(a) and 2(b) that organic films coated on bubble surfaces significantly enhance the bubble backscattering but change the total scattering by only a small amount when the bubble size is >1 μm. This is consistent with the study of Meyer[56] who found that the membrane of biological cells strongly influences the backscattering of radiation but does not significantly affect the forward scattering.

B. Mean Optical Efficiencies of Bubble Population

In principle, the bulk optical properties of bubble populations can now be estimated with Eq. (1) by using the generalized bubble size distributions (DI and DII) and the single-bubble efficiency factors computed above.

However, a more simplified case for bubble populations can be expected by transforming Eq. (2) into

$$j = N_0 \overline{Q_j}\, \bar{s}, \tag{6}$$

where

$$\overline{Q_j} = \frac{\int_{r_{\min}}^{r_{\max}} Q_j(r) p(r) \pi r^2 \mathrm{d}r}{\int_{r_{\min}}^{r_{\max}} p(r) \pi r^2 \mathrm{d}r}, \tag{7}$$

$$\bar{s} = \int_{r_{\min}}^{r_{\max}} p(r) \pi r^2 \mathrm{d}r. \tag{8}$$

$\overline{Q_j}$ and $\bar{s}$ are, respectively, the mean optical efficiency factors and the mean geometric cross-sectional areas of the bubble population. By use of Eq. (6), the influence of the bubble size distribution [or PDF, Eq. (2)] on bubble bulk optical properties was divided into two parts: the mean optical properties (efficiency factors) and the mean geometric property (mean area). Another advantage of doing so is that the mean optical properties of a population or culture are experimentally accessible, facilitating direct comparison with observations.

1. Clean Bubbles

Figure 3 shows (a) the mean scattering and (b) the backscattering efficiency factors for the DI (solid curves) and DII (dashed curves) bubble distributions as a function of mean radius $\bar{r} = \int_{r_{\min}}^{r_{\max}} rp(r)\mathrm{d}r$ for λ = 550 nm. For comparison, the respective efficiency factors for single bubbles are also displayed as a dotted curve in Figs. 3(a) and 3(b). Because the DI distribution is determined by both r_a and r_b [Eq. (4)], the mean efficiency factors are plotted for various r_a and r_b pairs (r_a = 0, 20, 40, 60, 80, and 100% of r_b). The fluctuation of efficiency factors seen in the single-bubble case has been largely damped out by the bubble population average. Only the first maximum and first minimum remain discernible, however with diminished amplitude.

It is interesting to note that for both scattering and backscattering efficiency factors, DII is not significantly different from the DI distribution with $r_a = r_b$ for a given mean radius. There are no systematic differences among various DI and between DI and DII distributions in forming the mean optical efficiency factors. This is because (1) the bubble size range is large so that the variations found in optical efficiency factors for single bubbles have been largely averaged out; and (2) for large bubbles [$r > 1$ μm, Figs. 2(a) and 2(b)], the scattering and backscattering efficiencies are stable, whereas the contribution of small bubbles rapidly decreases as the radius decreases ($Q_b \sim r^4$ if $r \ll \lambda$). It is therefore expected from Fig. 3 that the error might be small when one uses a single distribution to approximate the others in calculating the mean optical efficiency factors.

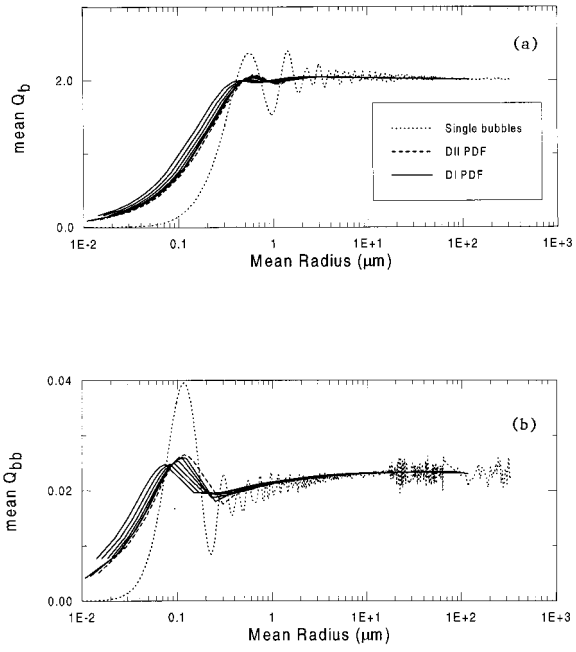

Fig. 3. (a) Mean scattering and (b) backscattering efficiencies of clean bubbles as a function of mean bubble radius for DI and DII bubble size distributions. DI (solid curves) from left to right correspond to r_a = 0, 0.2, 0.4, 0.6, 0.8, 1.0 r_b. Also shown as dotted curves are the efficiency factors of single clean bubbles for reference.

The errors that occur for tiny bubbles ($\bar{r} < 0.1$ μm) and for wide peaks ($r_a < 40\%$ of r_b) are less than 30%. There is virtually no error when $\bar{r} > 4$ μm. For the bubble populations observed in situ either by optical or acoustical methods, the mean radius is above 10 μm (Table 1, column 11), and therefore the mean scattering efficiency of these bubbles will depend only on the mean bubble radius, no matter what form the size distribution of the bubbles takes. The mean backscattering efficiency for clean bubbles calculated with this generalized bubble size distribution for $\bar{r} >$ 1 μm is ~0.02.

2. Dirty Bubbles

The influence of organic coatings on the mean scattering is shown in Fig. 4(a) and Fig. 4(b) shows backscattering efficiencies of bubble populations represented by DII with r_a = 60% of r_b. The mean total scattering efficiency [Fig. 4(a)], compared with that of clean bubbles, decreases as proteinaceous film thickness increases from 0.001 to 0.05 μm by as much as 25%, then it reverses and increases as the film becomes thicker. Only when the thickness of film reaches approximately 1 μm does the mean total scattering efficiency for dirty bubbles exceed that for clean bubbles by more than 10%. The mean total scattering is not affected with thickness <0.01 μm. Relatively large variations occur for thicker films. Despite variations in film thickness of 3 orders of magnitude (0.001 ~ 1 μm), there is little change in the mean total scattering when bubble size exceeds 10 μm.

Contrary to the total scattering, the mean back-

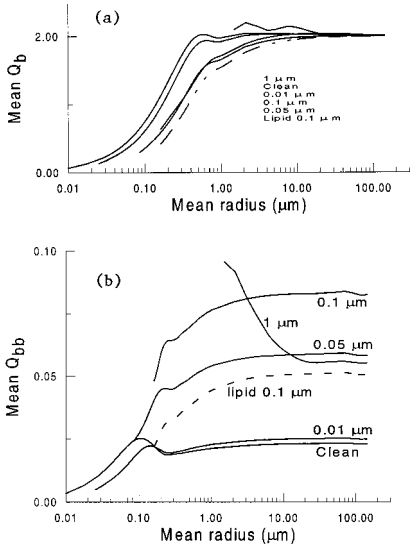

Fig. 4. (a) Mean scattering and (b) backscattering efficiencies of coated bubbles as a function of mean bubble radius and film thickness. From top to bottom, the scattering efficiencies for various coatings are indicated by the legend in the same order. For backscattering, the curves corresponding to various film thickness or composition are indicated individually.

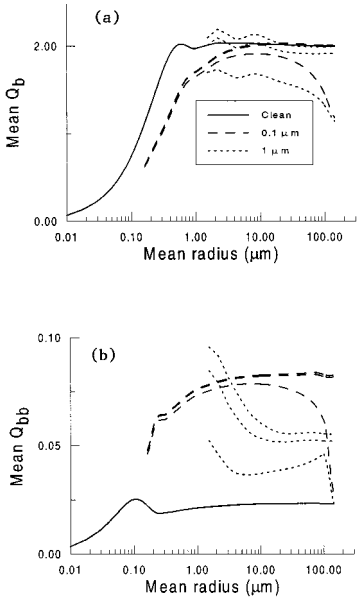

Fig. 5. Variations of (a) mean scattering and (b) backscattering efficiencies of coated bubbles with mean bubble radius as a function of thickness and imaginary index of the films. The solid curves are for clean bubbles, dashed curves for coated bubbles with 0.1-μm-thick film and dotted curves for 1-μm-thick film. Within a group, the curves from top to bottom represent efficiencies for bubbles with films without absorption, of imaginary index of 0.001, and of imaginary index of 0.006, respectively.

scattering experiences a variation of a factor of 5 in the presence of proteinaceous organic film. Except for bubbles coated with a 1-μm-thick film, the mean backscattering efficiency increases as film thickens ($\bar{r} > 0.2$ μm), with an enhancement of approximately 10% for 0.01-μm film to over four fold for 0.1-μm film.

The effects of different compositions of organic films are also shown in Figs. 4(a) and 4(b), where the mean scattering and backscattering efficiency factors for lipid film (index = 1.1) of thickness 0.1 μm are plotted by dashed curves. In general, the lipid film of the same thickness lowers both scattering and backscattering relative to the protein coatings. The reduction is more significant for backscattering than for scattering. With a lipid film of 0.1-μm thickness, scattering diminishes only 10%, whereas backscattering decreases by half in comparison with the protein coat.

It should be noted that in the above analysis, a constant layer thickness is applied regardless of the bubble size. Considering that the larger bubbles are only partially coated and that the coating of aged bubbles may be multilayered, the real situation in the ocean might be more complicated. Nevertheless, it is clear that coatings significantly increase the backscattering of bubble populations, especially for bubbles with a mean size of approximately 1–100 μm, the dominant sizes observed in the ocean (Table 1), even though the coating does not appear to have a strong influence on the total scattering of bubbles.

3. *Effect of Film Absorption*

There is only a small amount of data on the absorption properties of films coated onto the bubble surface. Here we estimate the imaginary part of the refractive index to be 0.001 and 0.006. The former is near the mean imaginary index of phytoplankton cells, whereas the latter is probably the maximum value for chlorophyll in the red absorption band.[57] Shown in Fig. 5 are the (a) mean scattering and (b) backscattering efficiency for bubbles coated with absorbing protein film. As expected, the absorption of organic film reduces both the total scattering and the backscattering, with the magnitude proportional to both thickness and the imaginary index of the film. Furthermore, the absorption also depends on the total bubble size, even though only the film has an absorbing property. However, only when the bubble sizes reach approximately 100 μm, and with an extremely high absorption coefficient (imaginary index = 0.006), does absorption significantly reduce the scattering and backscattering from the case with no absorption. It should be kept in mind that the imaginary index 0.006 tested here is the maximum value for the highly absorbing and colored substance chlorophyll.[57] For organic films with an imaginary index of 0.001, the reduced scattering and backscattering are at most 5%. Thus it is safe to say that the normally absorbing organic films exert a small influence on the backscattering of bubbles.

4. *Comparison with Plankton*

We can now compare the mean optical efficiency factors of bubble populations with those of autotrophic and heterotrophic plankton,[15,16,58] as listed in Table 2. The data for mean scattering and backscattering efficiencies are taken from Figs. 4(a) and 4(b) ($\bar{r} > 1$

Table 2. Mean Optical Efficiency Factors of Bubbles and Autotropic and Heterotrophic Plankton

	$\bar{d}$ μm	$\overline{Q}_b$	$\overline{Q}_{bb} \times 10^3$	$\tilde{b}_b \times 10^3$
Bubbles (1–300 μm)		1.5–2.2	22–82	11–200
Viruses[16] (30–150 nm)	0.072	5.16×10^{-4}	0.21	410
Bacteria[15,16] (0.1–1.5 μm)	0.55	0.10	1.00	10.0
Prochlorophytes[16] (0.6–0.8 μm)	0.8	0.22	1.40	6.36
Cyanobacteria[16] (0.5–3.0 μm)	0.8	0.61	1.39	2.28
Ultrananoplankton[16] (2–8 μm)	1.3	2.24	1.06	0.47
Flagellates[15] (2–6 μm)	4.2	2.0	0.6	0.30
Ciliates[15] (8–20 μm)	13.5	2.0	1.1	0.55
Larger nanoplankton[16] (8–20 μm)	11.1	1.79	1.97	1.10
Microplankton[16] (20–200 μm)	32.0	1.41	3.42	2.43

$\tilde{b}_b$ (backscattering ratio) = Q_{bb}/Q_b

μm), i.e., bubbles are assumed to be coated by an organic monolayer consisting of nonabsorbing protein or lipid. The mean scattering efficiency factor of bubbles (1.5–2.2) is comparable to those of nanoplankton (2–20 μm) and microplankton (20–200 μm). However, for the backscattering efficiency, ranging from 0.02 for clean bubbles to as high as 0.08 for bubbles with 0.1-μm-thick protein film, bubbles are at least 1 order of magnitude more efficient in backscattering than planktonic organisms, indicating the potential role of bubbles in regulating the ocean backscattering coefficient. It is due to their small size that the viruses and bacteria have the highest backscattering ratio (defined as the ratio of backscattering to total scattering) among autotrophic and heterotrophic plankton,[43] whereas the higher ratio for bubbles is by virtue of their refringent characteristics (m = 0.75).

C. Bulk Optical Properties of Bubble Populations

The bulk optical properties of natural bubble populations are calculated with the DI distribution with $r_a = 60\% r_b$ as a function of $\bar{r}$ for various bubble number densities (Fig. 6). For comparison, the total particulate scattering [Fig. 6(a)] and backscattering [Fig. 6(b)] coefficients are estimated as a function of pigment concentration through commonly used empirical relationships (e.g., Refs. 6, 16, 59):

$$b(\lambda) = \frac{550}{\lambda}(0.30 \pm 0.15)[\mathrm{Chl}]^{0.62} - b_w(\lambda), \qquad (9)$$

$$b_b(\lambda) = b(\lambda)\left[2 \times 10^{-3} + 2 \times 10^{-2} \times \left(0.5 - 0.25 \log_{10}([\mathrm{Chl}])\frac{550}{\lambda}\right)\right], \qquad (10)$$

and are plotted (dotted line) for [Chl] = 0.03 mg m^{-3} and (dashed line) [Chl] = 1 mg m^{-3}. Also shown are

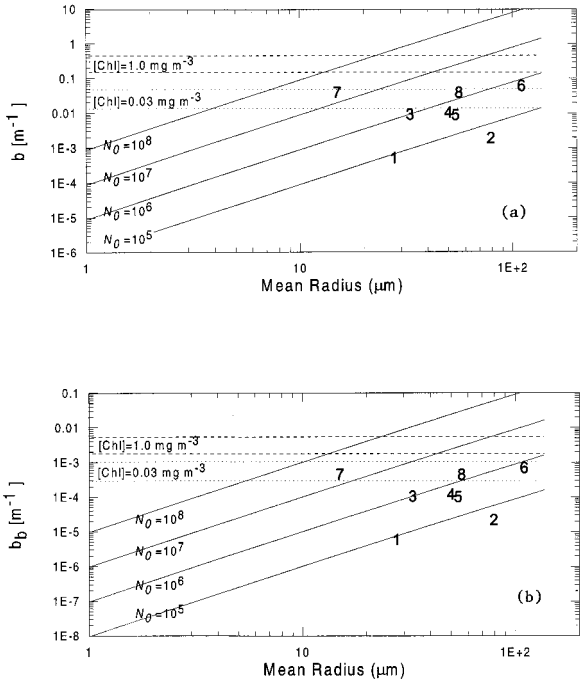

Fig. 6. (a) Scattering and (b) backscattering coefficients (solid lines) for clean bubble populations, represented by the generalized size distribution, as a function of mean bubble radius (in micrometers) (λ = 550 nm) for various bubble number densities. Also shown in numbers are the corresponding coefficients estimated with *in situ* observations (Table 1, column 1) based on the clean bubbles case. The two dashed lines are the upper and lower boundaries of coefficients calculated with Eq. (9) for Fig. 6(a) and Eq. (10) for Fig. 6(b) for [Chl] = 1 mg m^{-3}. The two dotted lines are for [Chl] = 0.03 mg m^{-3}.

total bubble scattering [Fig. 6(a)] and backscattering [Fig. 6(b)] coefficients estimated with Eq. (6) from *in situ* observations (Table 1, columns 13 and 14) and indicated by numbers corresponding to the serial number of Table 1 (column 1).

The backscattering coefficient that is due to the bubble populations from Table 1 range from 0.89–104% of total particle backscattering for [Chl] = 0.03 mg m^{-3} to 0.17–19% for [Chl] = 1 mg m^{-3}, whereas for scattering it is approximately 1.5–176% in oligotrophic water to 0.17–20% in eutrophic water. The largest case is from optical bubble measurements in the clear Tasman Sea.[39] Note that the scattering and backscattering coefficients estimated here for the bubble population are based on the clean bubbles only. From Figs. 4(a) and 4(b), we conclude that organic film absorbed onto bubbles would enhance the backscattering significantly, whereas it would change scattering only slightly. It is straightforward to extend the result to coated bubbles by multiplying the above estimates by a factor that can be inferred from Fig. 4(b). For example, the mean radius of the bubble populations observed *in situ* is approximately 50 μm and number density approximately 10^6 m^{-3} [Figs. 6(a) and 6(b), also Table 1]. Given such a bubble population, if the bubbles were clean they would contribute 16% to the particulate

backscattering for [Chl] = 0.1 mg m^{-3}; if the bubbles are coated with 0.1-μm-thick protein film they would account for 64%. For scattering there is almost no change with or without organic film for such a bubble population: The contribution is 28% of total scattering at the same chlorophyll concentration.

The study by Stramski[37] corresponds to point 7 in both Figs. 6(a) and 6(b); where our estimates are 4.51×10^{-4} m^{-1} for backscattering and 3.89×10^{-2} m^{-1} for scattering coefficients, which agrees well with Stramski's calculations ($b_b = 4.525 \times 10^{-4}$ m^{-1} and $b = 3.785 \times 10^{-2}$ m^{-1}) for high bubble concentration.

Based on the clean bubble case only, it can be seen that bubble populations play a significant role in modifying both scattering and backscattering coefficients if the mean radius is >10 μm and the bubble number density is $>10^7$ m^{-3}, or $r > 40$ μm, if N_0 reaches 10^7 m^{-3}, at least for the clear ocean. The organic film coating will enhance the backscattering considerably [Fig. 4(b)], and the contribution to the backscattering process will be highly significant even for eutrophic waters. The backscattering coefficient increases approximately three fold when chlorophyll concentration increases from 0.1 to 1 mg m^{-3}, whereas the backscattering of bubbles can be easily doubled or tripled by the coating, which occurs in seconds.[24]

D. Missing Terms in the Backscattering Process

Two almost simultaneous studies[15,16] concluded that all the effects that are due to phototrophic and heterotrophic organisms alone are not able to account for the observed total backscattering coefficient, and they argued that the missing terms in the backscattering process are probably attributed to the nonliving submicrometer detritus and/or viruses, a suggestion also contained in the early work by Brown and Gordon[18,19] and in the more recent study by Ulloa *et al.*[17] From Fig. 6(b), it is clear that the missing term could also include air bubbles if they were present in abundance, and if they had not been excluded when the *in situ* optical properties were measured. This is further exemplified by Fig. 7, where the total observed scattering and backscattering coefficient (solid line, upper and lower boundaries) is divided into contributions from phototrophic and heterotrophic organisms (dashed lines) plus that from clean bubbles ($\bar{r} = 50$ μm, $N_0 = 10^6$ and 10^7). The calculations of the scattering and backscattering coefficients of phototrophic and heterotrophic organisms are the same as that used by Morel and Ahn.[15] They assumed that the specific scattering coefficients for phototrophic organisms are 0.4, 0.2, and 0.1 m^2 (mg [Chl])$^{-1}$ for oligotrophic, mesotrophic, and eutrophic situations, respectively, and the backscattering ratio is 10^{-3}. For heterotrophic organisms represented by bacteria ($Q_b = 0.0886$, $Q_{bb} = 0.001$, $\bar{s} = 0.24$ μm^2), flagellate ($Q_b = 2.15$, $Q_{bb} = 0.0006$, $\bar{s} = 9.08$ μm^2), and ciliates ($Q_b = 1.85$, $Q_{bb} = 0.0011$, $\bar{s} = 143$ μm^2), they assumed the ratio of number density among bacteria, flagellate, and ciliates is $1:10^{-3}:10^{-5}$,

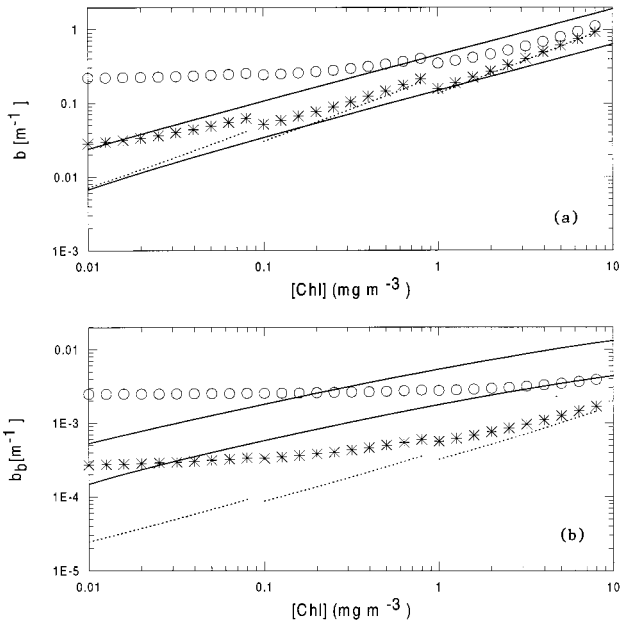

Fig. 7. Cumulative contributions (symbols) of bubbles and microorganisms (dashed lines) compared with *in situ* observed (a) scattering and (b) backscattering coefficients, represented by two solid lines corresponding to upper and lower boundaries of Eqs. (9) and (10), respectively. The bubbles are assumed to be clean, and their number density varies from 10^6 m^{-3} (*) to 10^7 m^{-3} (○). The backscattering that is due to micro-organisms alone could not account for the *in situ* measurements of backscattering.

and the number of bacteria depends on the chlorophyll *a* concentration through N_0 (bacteria) = $0.91 \times 10^{12} \times$ [Chl]$^{0.52}$.

By adding the scattering that is due to the resident clean bubble population, the large gap between values observed and estimated when taking into account only planktonic organisms can be filled, at least for the lower boundary. It is noted, however, that with $N_0 = 10^7$ m^{-3}, the reconstructed scattering [Fig. 7(a)] and backscattering coefficients [Fig. 7(b)] are even higher than that found in oligotrophic water ([Chl] = 0.01–0.1 mg m^{-3}).

It is curious that the empirical relationship given in Eq. (10) is evidently valid, given the low direct contribution to total backscattering by planktonic organisms. Although no relationship has ever been established between the number density of bubble populations and trophic state of the water where they are present, Thorpe *et al.*[60] found that the presence of particulates may enhance the number of smaller bubbles by their capture on the surface of the bubble and hence affect gas transfer and the rise speed. This is likely to be a significant factor in coastal waters and perhaps in the open ocean during bloom conditions. Their study suggested that there might be a connection between bubble density and the trophic state. Furthermore, oxygen evolved during photosynthesis might increase bubble densities. It is interesting to speculate that these connections may be responsible, albeit indirectly, for Eq. (9), and the subsequent development of semiempirical ocean color models.

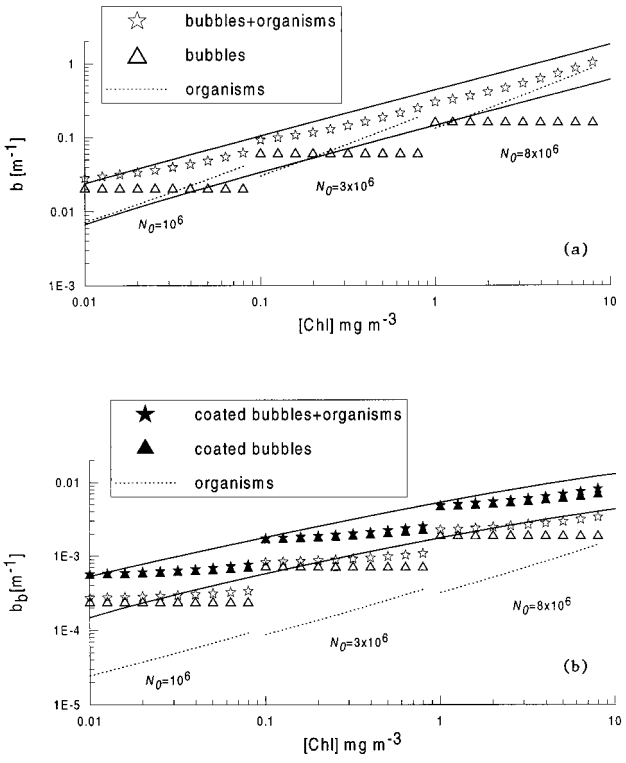

Fig. 8. Cumulative contributions (stars) of bubbles (triangles) and micro-organisms (dashed lines) as compared with *in situ* observed (a) scattering and (b) backscattering coefficients, represented by two solid lines corresponding to upper and lower boundaries of Eqs. (9) and (10), respectively. The bubble number density varies with the chlorophyll concentration, $N_0 = 10^6$, 3×10^6, and 8×10^6 m^{-3} for [Chl] = 0.01–0.1, 0.1–1, and 1.0–10 mg m^{-3}. The filled symbols correspond to the case in which the clean bubbles are replaced by dirty bubbles, which are assumed to increase the backscattering two fold according to Fig. 4.

As described above, previous studies[15,16] indicate that micro-organisms contribute little to particulate backscattering, but dominate the total scattering coefficient in the ocean. In the next analysis, we try to reconstruct the observed backscattering coefficient by including the bubble effect alone and simultaneously constrain the cumulative scattering coefficient within the observed range. The number density of the clean bubble population thus needed would be 0.6–1×10^6 for oligotrophic, 2–5×10^6 for mesotrophic, and 6–12×10^6 for eutrophic water. Such a case is shown in Fig. 8 [(a) for scattering coefficient and (b) for backscattering coefficient] with $N_0 = 10^6$, 3×10^6 and 8×10^6 for oligotrophic, mesotrophic, and eutrophic waters, respectively. From Table 1, it is apparent that these numbers are realistic, suggesting again that the contribution of bubble populations to backscattering, and hence remote-sensing reflectance [Eq. (1)], is significant. The large gap in the backscattering coefficient between the observed values and the estimated values that are due to micro-organisms can be filled by including contributions by bubbles while the summed scattering coefficient is consistent with *in situ* determinations. However, the recomposed backscattering coefficient based on clean bubbles covers only the lower boundary of observed backscattering values. Stramski and Kiefer[16] postulated that the missing term might be soft submicrometer detrital particles that that backscatter heavily but scatter considerably less. In reference to Table 2 and Fig. 4, we can argue that coated bubbles also have this property, a much enhanced backscattering efficiency with little change in the total scattering relative to clean bubbles. This effect is shown in Fig. 8 by solid symbols.

We conclude that the large missing terms in reconstructing the backscattering process can be easily explained by including a coated bubble population alone.

E. Influence on Remote Sensing

If bubbles persist in the ocean as described above, they contribute to the backscattering process and to *in situ* observations of the backscattering coefficients. These observations, which have been used empirically to establish the relationship between scattering and chlorophyll concentrations [Chl a] [Eqs. (9) and (10)], have already included any contribution by bubble populations, albeit implicitly (under the assumption that bubbles are still there when the measurements were being performed). The optical and biological properties that are derived with remote-sensing reflectance R [Eq. (1)] therefore are not influenced by the presence of these background bubble populations, because they are already accounted for at least for light to moderate wind conditions. However, a sudden injection of bubbles by, say, storm or ship wake, will influence the diffuse reflectance R by its enhanced backscattering.

Figure 9(a) shows the ratio of the enhanced diffuse reflectance R^B caused by injection of bubbles with a density of 10^6 and 10^7 m^{-3}, respectively, and with a mean radius of 50 μm to the normal diffuse reflectance R as a function of [Chl a]. The upper three curves are for bubbles with a number density of 10^7 m^{-3}, and 10^6 m^{-3} for the lower three. It is assumed that the bubbles are clean. For the coated bubble, the enhancement will be more significant according to Fig. 4(b). In general, the ratio R^B/R decreases as chlorophyll concentration increases because of an increase in scattering that is due to enhanced particulate content, and for a given [Chl a], the ratio increases with wavelength because the b_b for both clean and dirty bubbles are spectrally flat[61] whereas the b_b for ocean water decreases with wavelength [Eq. (10)]. Also because of this, injection of bubbles makes the ocean appear greener than before.

The change in color will further influence the optical and biological properties derived by use of the ratio of R at two wavelengths. Let OC denote the ratio of R at wavelengths 440 and 550 nm [OC = R(440 nm/R(550 nm)]. Figure 9(b) shows the variation of OC after the bubble injection relative to that before the bubble injection. The upper two curves are for bubbles with a number density of 10^6 m^{-3}, and 10^7 m^{-3} for the lower two. The coated bubbles are

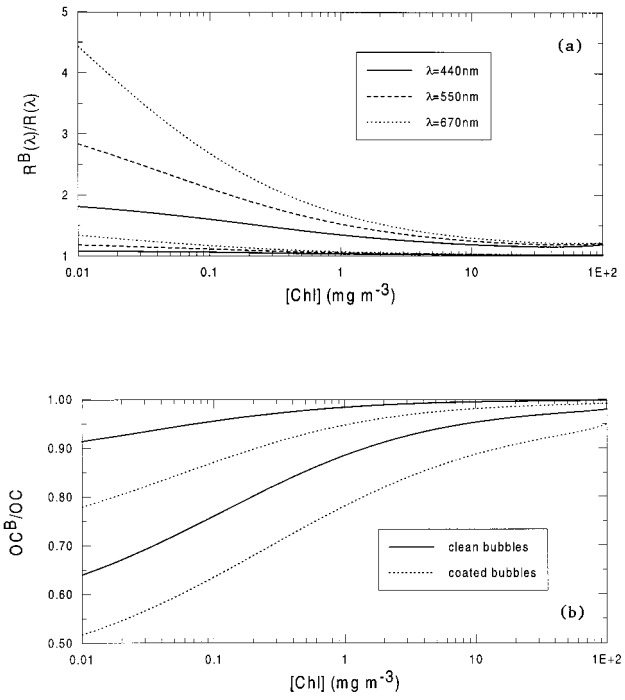

Fig. 9. (a) Ratio of enhanced diffuse reflectance R^B that is due to clean bubble injection to the normal reflectance R as a function of [Chl] for various wavelengths. The upper three curves are estimates obtained with clean bubbles having a number density of 10^7 m^{-3}, whereas the lower three use 10^6 m^{-3}. (b) The variation of OC^B after the bubble injection relative to OC before the bubble injection as a function of [Chl] for clean and coated bubbles (protein film of 0.1 μm). The upper two curves are for injected bubbles with a number density of 10^6 m^{-3}, and the lower two use 10^7 m^{-3}.

assumed to be coated with protein film of 0.1 μm. The color ratio decreases because of the bubble injection, and the change is more severe in open ocean than in coastal water.

The bubbles therefore influence the remote-sensing retrieval in two aspects. First, by overall increases in the backscattering at all wavelengths, the assumption of negligible reflectance in the red (or near IR) that is used by the ocean color atmospheric correction algorithm would be invalid. The water-leaving radiance or the remote-sensing reflectance in the shorter wavelengths would be underestimated if no corrections were to be made for the enhanced backscattering in the red or near IR that is due to bubbles. Second, the change in color translates into an error in the estimated remote-sensing products, for example, the chlorophyll concentration in open ocean will be overestimated from 10% for clean bubbles and $N_0 = 10^6$ m^{-3} to a factor of 2 for coated bubbles and $N_0 = 10^7$ m^{-3} according to Fig. 9(b). This is higher than the error budget (30%) for chlorophyll concentration derived from the SeaWIFS project.[62]

4. Conclusions

We applied Mie theory to estimate the optical efficiency factors for both clean and organic film-coated bubbles in the ocean and to study the effect of thickness and composition of this film coating on the light-scattering capability. Based on published *in situ* observations of bubbles in ocean water, a generalized bubble size distribution was proposed. By use of this generalized bubble size distribution, the optical properties, i.e., scattering and backscattering coefficients, of bubble populations were calculated and compared with the optical properties of natural particles as well as with the integrated observed scattering coefficients.

In the visible domain, there is no significant difference in total scattering between clean bubbles and bubbles coated with organic film (dirty bubbles). Bubbles coated with an organic film exhibit an enhanced backscattering efficiency that is due to coating. The enhancements, generally, are directly proportional to both the refractive index and the thickness of the film. For a bubble population with a mean radius greater than 1 μm, the backscattering efficiency can be enhanced by a factor of 4 because of organic coating of thickness of approximately 0.1 μm. The absorption (if any) that is due to the organic film on the surface of bubbles reduces both scattering and backscattering; however, this effect is negligible.

Given the bubble number density (from $\sim 10^5$ to $\sim 10^7$) that has typically been reported from measurements in the sea, the bubble population significantly influences the scattering process in the ocean, especially in oligotrophic waters. For the average bubble size distributions that have been reported ($N_0 = 10^6$ m^{-3} and $\bar{r} = 50$ μm) and for [Chl] = 0.1 mg m^{-3}, bubbles contribute 14–42% of total scattering.

By virtue of the refringent characteristics ($m = 0.75$), bubbles have a backscattering efficiency at least 1 order of magnitude higher than backscattering efficiencies reported for planktonic organisms (Table 2). The contribution of a bubble population ($N_0 = 10^6$ m^{-3} and $\bar{r} = 50$ μm) to the backscattering coefficient at [Chl] = 0.1 mg m^{-3} is 8–24% for clean bubbles and 30–100% for dirty bubbles with protein film of 0.1 μm thick. Thus backscattering from bubble populations is likely to be one of the missing terms in constructing the observed total backscattering coefficient in the sea. Obviously, this contribution to backscattering by bubbles is strongly enhanced if the bubbles are coated with organic film.

Through enhanced backscattering over the whole visible domain, the bubbles will influence the remote sensing of ocean color in (1) atmospheric correction and (2) optical and biological properties derived with color ratios. For high bubble concentrations, the assumption that there is negligible reflectance in red and near IR will be invalid. The ocean color tends to be greener because of bubbles, and the chlorophyll concentration would, therefore, be overestimated.

In conclusion, bubbles are strong scatterers and backscatterers whose influence on ocean optics and remote sensing has long been neglected. Caution should therefore be taken when trying to interpret the remote-sensing reflectance ($\sim b_b/a$) and in the decomposition of the total scattering or backscattering coefficient into constituent contributions. On the other hand, more intensive and extensive efforts

should be directed to a better understanding of the expected variability in the bubble size distribution and its possible relationship with the trophic state.

The authors gratefully acknowledge the U.S. Office of Naval Research and the Canadian Natural Sciences and Engineering Research Council for their support, and A. Morel and D. Stramski for constructive reviews.

References and Notes

1. R. C. Dugdale, A. Morel, A. Bricaud, and F. P. Wilkerson, "Modeling new production in upwelling centers: a case study of modeling new production from remotely sensed temperature and color," J. Geophys. Res. **94,** 18,119–18,132 (1989).
2. T. Platt, C. Caverhill, and S. Sathyendranath, "Basin-scale estimates of oceanic primary production by remote sensing: the North Atlantic." J. Geophys. Res. **96,** 15,147–15,160 (1991).
3. M. R. Lewis, "Satellite ocean color observations of global biogeochemical cycles," in Primary Productivity and Biogeochemical Cycles in the Sea, P. G. Falkowski and A. Woodhead, eds. (Plenum, New York, 1992), pp. 139–154.
4. H. R. Gordon, O. B. Brown, and M. M. Jacobs, "Computed relationships between the inherent and apparent optical properties of a flat homogeneous ocean," Appl. Opt. **14,** 417–427 (1975).
5. A. Morel and L. Prieur, "Analysis of variations in ocean color," Limnol. Oceanogr. **22,** 709–722 (1977).
6. H. R. Gordon and A. Morel, Remote Assessment of Ocean Color for Interpretation of Satellite Visible Imagery, a Review (Springer-Verlag, New York, 1983).
7. A. Morel and B. Gentili, "Diffuse reflectance of oceanic waters: its dependence on Sun angle as influenced by the molecular scattering contribution," Appl. Opt. **30,** 4427–4438 (1991).
8. A. Morel and B. Gentili, "Diffuse reflectance of oceanic waters: III. Implication of bidirectionality for the remote-sensing problem," Appl. Opt. **35,** 4850–4862 (1996).
9. H. R. Gordon, O. B. Brown, R. H. Evans, J. W. Brown, R. C. Smith, K. S. Baker, and D. K. Clark, "A semi-analytical radiance model of ocean color," J. Geophys. Res. **93D,** 10,909–10,924 (1988).
10. A. Morel, "Optical modeling of upper ocean in relation to its biogenous matter content (case I waters)," J. Geophys. Res. **48,** 145–175 (1988).
11. A. Bricaud, M. Babin, A. Morel, and H. Claustre, "Variability in the chlorophyll-specific absorption coefficients of natural phytoplankton: analysis and parameterization," J. Geophys. Res. **100,** 13,321–13,332 (1995).
12. J. S. Cleveland, "Regional models for phytoplankton absorption as a function of chlorophyll a concentration," J. Geophys. Res. **100,** 13,333–13,344 (1995).
13. A. Morel and A. Bricaud, "Theoretical results concerning the optics of phytoplankton, with special reference to remote sensing applications," in Oceanography from Space, J. F. R. Gower, ed. (Plenum, New York, 1981), pp. 313–327.
14. Y. Ahn, A. Bricaud, and A. Morel, "Light backscattering efficiency and related properties of some phytoplankters," Deep-Sea Res. **39,** 1835–1855 (1992).
15. A. Morel and Y. Ahn, "Optics of heterotrophic nanoflagellates and ciliates: a tentative assessment of their scattering role in oceanic waters compared to those of bacterial and algal cells," J. Mar. Res. **49,** 177–202 (1991).
16. D. Stramski and D. A. Kiefer, "Light scattering by microorganisms in the open ocean," Prog. Oceanogr. **28,** 343–383 (1991).
17. O. Ulloa, S. Sathyendranath, and T. Platt, "Effect of the particle-size distribution on the backscattering ratio in seawater," Appl. Opt. **33,** 7070–7077 (1994).
18. O. B. Brown and H. R. Gordon, "Two component Mie scattering models of Sargasso Sea particles," Limnol. Oceanogr. **17,** 826–832 (1973).
19. O. B. Brown and H. R. Gordon, "Size-refractive index distribution of clear coastal water particulates from light scattering," Appl. Opt. **13,** 2874–2881 (1974).
20. B. D. Johnson and R. C. Cooke, "Bubble populations and spectra in coastal waters: a photographic approach," J. Geophys. Res. **84,** 3761–3766 (1979).
21. H. Medwin and N. D. Breitz, "Ambient and transient bubble spectral densities in quiescent seas and under spilling breaker," J. Geophys. Res. **94,** 12,751–12,759 (1989).
22. T. J. O'Hern, L. d'Agostino, and A. J. Acosta, "Comparison of holographic and coulter counter measurement of cavitation nuclei in the ocean," Trans. ASME J. Fluids Eng. **110,** 200–207 (1988).
23. D. C. Blanchard and A. H. Woodcock, "Bubble formation and modification in the sea and its meteorological significance," Tellus **9,** 145–158 (1957).
24. S. A. Thorpe, "On the clouds of bubbles formed by breaking wind-waves in deep water, and their role in air-sea gas transfer," Philos. Trans. R. Soc. London Ser. A **304,** 155–210 (1982).
25. D. M. Farmer, C. L. McNeil, and B. D. Johnson, "Evidence for the importance of bubbles in increasing air-sea gas flux," Nature (London) **361,** 620–623 (1993).
26. H. Medwin, "In situ acoustic measurements of bubble populations in coastal ocean waters," *J. Geophys. Res.* **75,** 599–611 (1970).
27. H. Medwin, "In situ acoustic measurements of microbubbles at sea," J. Geophys. Res. **82,** 971–976 (1977).
28. E. C. Monahan, "The ocean as a source for atmospheric particles," in The Role of Air-Sea Exchange in Geochemical Cycling, P. Buat-Menard, ed. (Reidel, Dordrecht, The Netherlands, 1986), pp. 129–163.
29. D. C. Blanchard and L. D. Syzdek, "Film drop production as a function of bubble size," J. Geophys. Res. **93,** 3649–3654 (1988).
30. J. Wu, "Bubble populations and spectra in near-surface ocean: summary and review of field measurements," J. Geophys. Res. **86,** 457–463 (1981).
31. P. L. Marston and D. L. Kingsbury, "Scattering by a bubble in water near the critical angle: interference effects," J. Opt. Soc. Am. **71,** 192–196 (1981).
32. D. L. Kingsbury and P. L. Marston, "Mie scattering near the critical angle of bubbles in water," J. Opt. Soc. Am. **71,** 358–361 (1981).
33. P. L. Marston, D. S. Langley, and D. L. Kingsbury, "Light scattering by bubbles in liquids: Mie theory, physical-optics approximations, and experiments," Appl. Sci. Res. **38,** 373–383 (1982).
34. P. L. Marston, S. Billette, and C. Dean, "Scattering of light by a coated bubble in water near the critical and Brewster scattering angles," in *Ocean Optics IX*, M. A. Blizard, ed., Proc. SPIE **925,** 308–316 (1988).
35. W. Arnott and P. L. Marston, "Optical glory of small freely rising gas bubbles in water: observed and computed cross-polarized backscattering patterns," J. Opt. Soc. Am. A **5,** 496–506 (1988).
36. W. Arnott and P. L. Marston, "Unfolded optical glory of spheroids: backscattering of laser light from freely rising spheroidal air bubbles in water," Appl. Opt. **30,** 3429–3442 (1991).
37. D. Stramski, "Gas microbubbles: an assessment of their significance to light scattering in quiescent seas," in *Ocean Optics XII*, J. S. Jaffe, eds., Proc. SPIE **2258,** 704–710 (1994).

38. D. A. Kolovayev, "Investigation of the concentration and statistical size distribution of wind-produced bubbles in the near-surface ocean," Oceanology **15,** 659–661 (1976).
39. A. L. Walsh and P. J. Mulhearn, "Photographic measurements of bubble populations from breaking wind waves at sea," J. Geophys. Res. **92,** 14,553–14,565 (1987).
40. G. De Leeuw and L. H. Cohen, "Bubble size distribution in coastal seas," in Air-Water Gas Transfer, B. Jahne and E. C. Monahan, eds. (AEON Verlag and Studio, Hanau, Germany, 1995) pp. 325–336.
41. R. E. Glazman, "Effects of adsorbed films on gas bubble radial oscillations," J. Acoust. Soc. Am. **74,** 980–986 (1983).
42. C. F. Bohren and D. R. Huffman, Absorption and Scattering of Light by Small Particles (Wiley, New York, 1983).
43. H. C. van de Hulst, Light Scattering by Small Particles (Wiley, New York, 1957).
44. B. D. Johnson and R. C. Cooke, "Generation of stabilized microbubbles in seawater," Science **213,** 209–211 (1981).
45. D. E. Yount, E. W. Gillary, and D. C. Hoffman, "A microscopic investigation of bubble formation nuclei," J. Acoust. Soc. Am. **76,** 1511–1521 (1984).
46. D. E. Yount, "Skins of varying permeability: a stabilization mechanism for gas cavitation nuclei," J. Acoust. Soc. Am. **65,** 1429–1439 (1979).
47. E. C. Monahan, "Near surface bubble concentration and oceanic whitecap coverage," in Seventh Conference on Ocean-Atmosphere Interaction (American Meteorological Society, Boston, Mass., 1988), pp. 178–181.
48. J. Wu, "Bubble flux and marine aerosol spectra under various wind velocities," J. Geophys. Res. **97,** 2327–2333 (1992).
49. J. Wu, "Bubbles in the near-surface ocean: a general description," J. Geophys. Res. **93,** 587–590 (1988).
50. B. D. Johnson, "Bubble populations: background and breaking waves," in Oceanic Whitecaps and Their Role in Air-Sea Exchange Processes, E. C. Monahan and G. Mac Niocaill, eds. (Reidel, Dordrecht, The Netherlands, 1986), pp. 69–73.
51. F. MacIntyre, "On reconciling optical and acoustical bubble spectra in the mixed layer," in Oceanic Whitecaps and Their Role in Air-Sea Exchange Processes, E. C. Monahan and G. Mac Niocaill, eds. (Reidel, Dordrecht, The Netherlands, 1986), pp. 75–94.
52. G. B. Crawford and D. M. Farmer, "On the spatial distribution of ocean bubbles," J. Geophys. Res. **92,** 8231–8243 (1987).
53. P. J. Mulhearn, "Distribution of microbubbles in coastal waters," J. Geophys. Res. **86,** 6429–6434 (1981).
54. B. D. Johnson and P. J. Wangersky, "Microbubbles: stabilization by monolayers of adsorbed particles," J. Geophys. Res. **92,** 14,641–14,647 (1987).
55. F. E. Fox and K. Herzfeld, "Gas bubbles with organic skin as cavitation nuclei," J. Acoust. Soc. Am. **26,** 984–989 (1954).
56. R. A. Meyer, "Light scattering from biological cells: dependence of backscattering radiation on membrane thickness and refractive index," Appl. Opt. **18,** 585–588 (1979).
57. A. Morel, "Optics of marine particles and marine optics," in Particle Analysis in Oceanography, S. Demers, ed. (Springer-Verlag, Berlin, 1990), pp. 141–188.
58. A. Morel and Y. Ahn, "Optical efficiency factors of free-living marine bacteria: influence of bacterioplankton upon the optical properties and particulate organic carbon in oceanic waters," J. Mar. Res. **48,** 145–175 (1990).
59. C. D. Mobley, Light and Water: Radiative Transfer in Natural Waters (Academic, New York, 1994).
60. S. A. Thorpe, P. Bowyer, and D. K. Woolf, "Some factors affecting the size distributions of oceanic bubbles," J. Phys. Oceanogr. **22,** 382–389 (1992).
61. According to Mie theory, the optical efficiency depends only on refractive index and a size factor $x = 2\pi r/\lambda$, where r is the particle radius and λ is the wavelength. They have an equivalent but reverse effect on x. For example, that the optical efficiency is constant in the visible (400–700 nm) at $r = 50$ μm only requires that it does not change for r from 39 to 69 μm at $\lambda = 550$ nm. For backscattering coefficient of bubbles, this requirement is almost always satisfied for both clean and dirty bubbles (Fig. 4).
62. S. B. Hooker, W. E. Esaias, G. C. Feldman, W. W. Gregg, and C. R. McClain, "An overview of SeaWiFS and ocean color," in SeaWiFS Technical Report Series, Vol. 1, NASA Tech. Memo. 104566 (NASA, Greenbelt, Md., 1992).